Rapid Communications

Efficient coupling of disorder states to excitons in an InGaN nanostructure

Cameron Nelson,[1,2] Yong-Ho Ra,[3] Zetian Mi,[1] and Duncan G. Steel[1,2]

[1]*Center for Photonics and Multiscale Materials, University of Michigan, Ann Arbor, Michigan 48109, USA*

[2]*H. M. Randall Laboratory of Physics, University of Michigan, Ann Arbor, Michigan 48109, USA*

[3]*Department of Electrical and Computer Engineering, McGill University, 3480 University Street, Montreal, Quebec, Canada H3A 0E9*

(Received 16 June 2018; published 13 August 2018)

$In_xGa_{1-x}N$ disks in GaN nanowires (DINWs) have emerged as a viable technology for on-chip tunable visible spectrum emission without the use of a phosphor. Here, we present a study of the optical emission and absorption dynamics in DINWs that incorporates the important role of background disorder states. The optical emission in the system is dominated by quantum-confined excitons, however, we show here that the excitons are coupled to a large density of background disorder states. Rapid nonradiative decay (compared to other decay rates such as spontaneous emission) from disorder states into excitons is observed after optical excitation of our sample that dominates the nonlinear absorption dynamics. Because disorder states are ubiquitous in InGaN layers, we believe that this result reveals an important decay channel that should be incorporated in future modeling and engineering of InGaN-based optical devices in general.

DOI: 10.1103/PhysRevB.98.081201

Epitaxially grown planar $In_xGa_{1-x}N$/GaN layers have become an industry standard for solid state white light emitters such as light-emitting diodes (LEDs). In conventional planar quantum well structures, achieving efficient full visible spectrum emission has been challenging due to issues such as efficiency droop at high injection currents [1], large internal polarization fields [2,3], and a rapidly decreasing emission efficiency as a function of increasing InN concentration, known as the green gap [4–6].

Many of the above issues have been mitigated in InGaN disk-in-nanowire (DINW) structures that can be grown defect-free on foreign substrates such as Si [7] with significantly reduced internal electric fields due to strain relaxation in the active area [8,9]. These improvements have paved the way for recent demonstrations such as on-chip full visible spectrum lasers [10,11] and red-green-blue LED arrays [7,12–14]. Smaller diameter (∼100-200 nm or less) DINWs support emission from exciton states (Coulomb-bound electron-hole pairs) that are confined to the center of the InGaN disk due to strain relaxation at the DINW sidewalls [2,9,14–16]. Because of bright emission from the quantum-confined excitons, devices made from DINWs have shown the potential for large increases in emission efficiency over more conventional planar InGaN quantum well devices at all wavelengths [2,9,14–16]. Excitons that are confined to the center of the DINW in three dimensions have also become a promising candidate for quantum information science applications such as high-temperature single-photon emitters [15]. Hence, understanding the excited states and relation pathways for injected carriers is important for understanding the fundamental limits for the quantum yield as well as for being able to evaluate these structures for possible applications to advanced devices for quantum information.

Studies of InGaN layers over the last few decades have often been focused on understanding the physics of disorder in InGaN layers. Electronic energy states formed by disorder arise naturally in InGaN systems from random variations in the InN concentration within the material or from atomistic defects [17–19] such as In-N-In chains [19]. The important role of disorder states is highlighted in planar InGaN quantum well light emitters, where excitonic emission is typically quenched due to a large density of threading defects in the active region that are not present in DINWs [8,17]. Emission in planar quantum wells is instead provided by radiative recombination of electron-hole pairs trapped by localized disorder states that are small enough to avoid the defect sites [17]. Recent results have confirmed that large densities of disorder states can also exist in DINW systems [20], although, as noted above, the emission from DINWs has been shown to be dominated by radiative recombination from quantum-confined exciton states rather than localized disorder states.

Currently the combined dynamics of optically excited excitons and disorder states including effects such as population transfer via nonradiative decay of electron-hole pairs has not been characterized in InGaN systems. As optical devices continue to utilize emission from quantum-confined excitons using DINWs and other structures such as self-assembled quantum dots, it will become more important to understand the physics of exciton-disorder state systems.

In this Rapid Communication, we study the linear and nonlinear optical properties of an ensemble of red-emitting, selective area InGaN/GaN DINWs that support emission from quantum-confined excitons in order to understand the physical processes in the system associated with optically excited disorder states and excitons. Using coherent pump probe (CPP), photoluminescence (PL), and photoluminescence excitation (PLE) spectroscopy data along with a model of the system based on the optical Bloch equations, we find that the dynamics of optically excited electron-hole pairs can be described using incoherent coupling between optically excited electron-hole pairs in the background disorder states and the quantum-confined exciton states. Measurements such as PL are

dominated by processes in which electron-hole pairs are first excited into the background disorder states (in first and second order of perturbation theory in our model), then subsequently decay into the exciton states (resulting in a nonlinear absorption signal to third order). This finding suggests that optical excitation of background disorder can effectively increase the PL brightness of excitons in the system by providing a higher rate of exciton state filling compared to systems with no disorder.

Experiments were performed on an ensemble of site-defined InGaN disks in GaN nanowires grown on a GaN template on a sapphire substrate using plasma-assisted molecular beam epitaxy (PAMBE). Each nanowire contains ∼600 nm GaN, eight InGaN(3 nm)/GaN(3 nm) vertically aligned quantum disks, and a ∼5-nm GaN capping layer. Further details of the growth procedure are discussed in the Supplemental Material [21] and references therein [12,22]. The PL and PLE spectra of the sample (excitation spot size ∼1 μm^2, exciting ∼200-300 DINWs) are shown in Fig. 1(a). To collect PL data, the sample is excited in a backward geometry by a continuous-wave 3.06-eV diode laser. This laser is replaced by a tunable laser for PLE measurements. The PL spectrum (black) shows a broad resonance while the PLE spectrum (red) is dominated by a relatively featureless signal that is closely described by an exponential function of energy, as noted earlier. The apparent exponential energy dependence of the PLE spectrum below the band edge is a common signature of inhomogeneous broadening from disorder states that has been observed frequently in InGaN systems [23–25]. It is typical for the linear absorption spectrum in InGaN systems to be dominated by a large density of disorder states rather than excitons, where the density of disorder (and the length of the tail) increases with increasing InN concentration [24].

To perform CPP measurements, the differential transmission (dT/T, where T is the sample transmittance) of a tunable probe beam is monitored to detect the changes in sample absorption properties induced by a separately tunable pump beam using phase-sensitive detection. The lowest-order contribution to the differential transmission signal of interest is proportional to the imaginary component of the third-order [in the field, $\chi^{(3)}(\omega_{\text{probe}} = \omega_{\text{probe}} + \omega_{\text{pump}} - \omega_{\text{pump}})$, where ω is the optical frequency] nonlinear optical response of the sample. Further details of the detection technique are discussed in the Supplemental Material [21].

The degenerate CPP (DCPP, $\omega_{\text{pump}} = \omega_{\text{probe}}$) data [shown in Fig. 1(b)] show a series of resonances that are peaked in amplitude around 2.05 eV and slowly roll off as a function of energy. Similar results from previous studies have been observed [20,26], where the resonant structures in the degenerate nonlinear absorption spectrum were assigned to exciton transitions. Here, we attribute the resonances to quantum-confined exciton states from different-sized DINWs within the ensemble, an assignment that will be further validated shortly. Energy separations between the exciton states are ∼10's of meV and can be accounted for by the variation in DINW diameter due to the tapered design of the DINW [12] or possibly from excited-state transitions in the system [9]. We rule out that the resonances observed in the nonlinear spectrum are due to étalon effects because the DCPP data show similar resonances to the modulated absorption [27] spectrum of the sample (not shown), where the pump beam is replaced by a 3.06-eV diode. In this measurement, such an étalon effect would depend strongly on the pump energy since the nonlinear signal (dT/T) is normalized to the probe transmission and no strong pump energy dependence of the resonances has been observed.

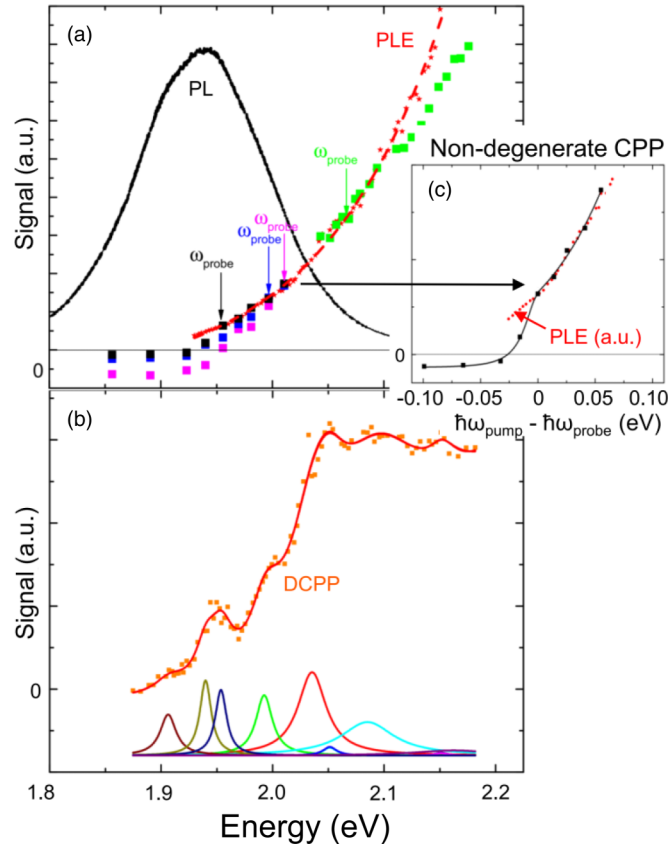

FIG. 1. (a) PL spectrum (black) plotted with PLE (red), and several nondegenerate CPP spectra with fixed probe energy and scanning pump. The PLE spectrum is fit using a single Lorentzian. The fixed probe energies are shown by the solid arrows. For each fixed probe energy, the corresponding nondegenerate CPP spectrum is color coded to match the solid arrow. The data are individually normalized to facilitate comparison of the qualitative behavior. The nondegenerate CPP data are scaled so that the $\omega_{\text{pump}} = \omega_{\text{probe}}$ point coincides with the PLE spectrum. (b) Degenerate CPP ($\omega_{\text{pump}} = \omega_{\text{probe}}$) fit with a total of nine exponentially weighted Lorentzians as per Eq. (S9) from the Supplemental Material [21]. (c) Nondegenerate CPP data for a fixed probe energy of 1.95 eV fitted to the indirect term from Eq. (S9) from the Supplemental Material [21] (black points and line) along with the PLE data (red points) plotted as a function of pump-probe detuning.

The nondegenerate CPP data for fixed probe beam energies and as a function of scanning pump energy are also shown in Fig. 1(a). We find that the saturation of the probe absorption due to the presence of the pump (positive dT/T) increases rapidly as a function of energy for $\omega_{\text{pump}} \geqslant \omega_{\text{probe}}$ and shows a qualitatively similar dependence on energy as the PLE spectrum. For $\omega_{\text{probe}} > \omega_{\text{pump}}$, the CPP signal tends to decrease more rapidly than the PLE signal and has an additional negative dT/T (an increase in absorption) offset that is observed once the pump beam is sufficiently detuned from the probe. The

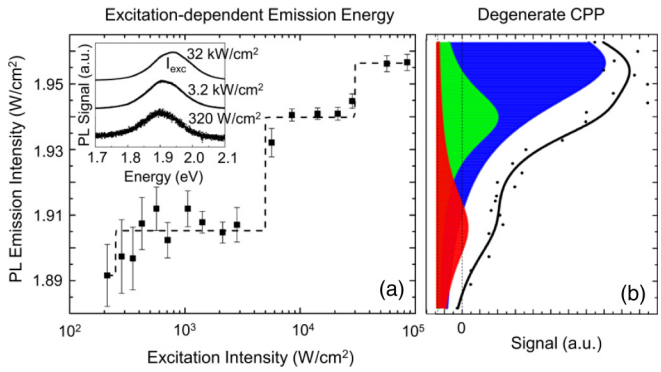

FIG. 2. (a) PL peak energy plotted as a function of excitation intensity. The error bars represent variation in the measurement possibly caused by small sample vibrations. The inset shows the PL spectrum for three different orders of magnitude in excitation intensity. The dashed line is a fit to the simple model. (b) DCPP spectrum with a 3-Lorentzian fit in the same energy window as shown in (a). The peak energy of the Lorentzians is the same energy as the excitation intensity-independent regions in (a).

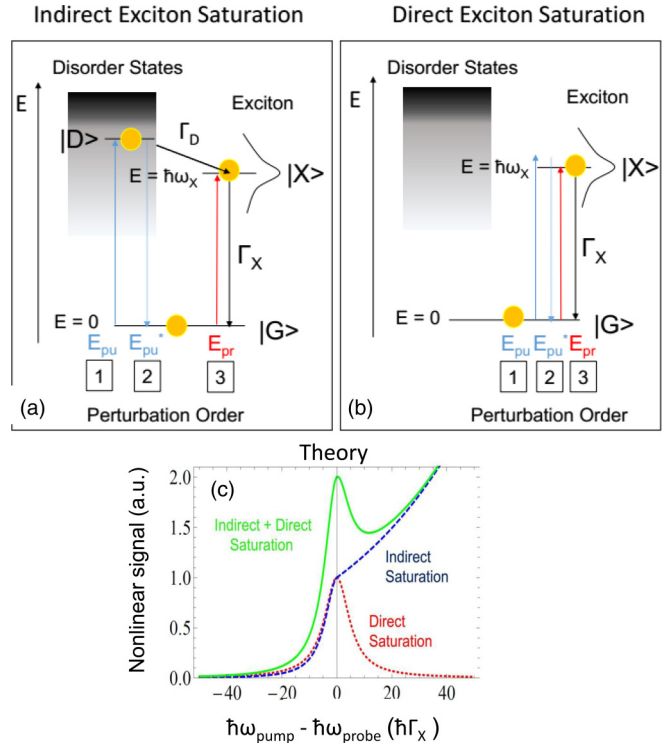

FIG. 3. (a) Model for the energy levels in the system along with the perturbation sequence for indirect exciton saturation. The exciton state is represented by $|X\rangle$ with energy $\hbar\omega_X$ while the disorder states that are resonant with the pump beam are represented by $|D\rangle$. The yellow circles represent states that have a nonzero population of electron-hole pairs in second order. (b) Corresponding energy-level diagram and perturbation sequence for direct exciton saturation. (c) Theoretical nonlinear response from the imaginary part of Eq. (S9) from the Supplemental Material [21]. The indirect term [first term on the right-hand side of Eq. (S9) and corresponding terms in Eqs. (S10) and (S11) (green dashed)] is shown separately from the direct term [second on the right-hand side of Eq. (S9) (red dots)].

measurement is repeated for several different fixed probe energies and the same qualitative behavior is observed in each case, however, the magnitude of the negative dT/T background signal generally increases as a function of fixed probe energy. A negative dT/T offset has been observed in previous nonlinear spectroscopy studies of self-assembled DINW samples [20]. The origin of the negative offset, which can be observed in degenerate CPP spectra as well, is still under investigation, however, it may be an effect related to band-gap renormalization or screening [20,28,29]. A zoomed-in view of the nondegenerate CPP spectrum for a fixed probe near 1.95 eV is shown in Fig. 1(c) along with the PLE spectrum. The data are fit using a model based on the optical Bloch equations and will be discussed further later on. In addition to the above nonlinear optical data, the CPP spectrum also features narrow (sub-μeV) resonances at zero pump-probe detuning that are caused by coherent population pulsations (not shown). The nature of the population pulsation resonances has been explored in a previous work featuring an identical sample at room temperature [30].

To further understand the system, we consider the intensity-dependent PL spectrum as shown in Fig. 2(a). It has been shown that emission from exciton states in individual, localized DINW systems shows no energy shift as a function of excitation intensity and effects such as charge screening of the internal electric fields that would result in carrier density-dependent shifts are insignificant [2,31]. The energy-independent regions of Fig. 2(a) are therefore consistent with emission from exciton states, where the energy differences can be provided by the DINW diameter [12]. The discrete blueshifting behavior in Fig. 2(a) is contrary to simple two-level dynamics but can be accounted for in the model discussed in the Supplemental Material [21,32] and is related to the variation in emission energies and PL saturation intensities in the system from groups of DINWs with different diameters, as observed in Ref. [12]. As a simple approximation, we find that the DCPP data can be fit to a series of Lorentzians (note that this simple approach will be modified later on), each representing nonlinear absorption from exciton transitions. We find that the center energy of the Lorentzians from the fit in Fig. 2(b) shows good agreement with the excitation intensity-independent energies from Fig. 2(a). These data show a consistency in our interpretation of the nonlinear absorption signal being mainly sensitive to exciton states rather than absorption from the disorder states.

To understand the nondegenerate nonlinear data, we consider a unified model of the system in which electron-hole pairs can be excited into background disorder states and subsequently decay nonradiatively into lower-energy exciton states. The nonradiative decay process could occur from the emission of acoustic phonons, for example [33,34]. In our model, the probe beam is also resonant with a homogeneously broadened exciton state $|X\rangle$ and that the pump beam is allowed to vary in energy. In the Supplemental Material, the third-order signal is found using the above model and the optical modified Bloch equations to third order in perturbation theory [21,32]. We consider two different excitation pathways that contribute to the third-order signal: The first represents excitation of electron-hole pairs in the background disorder states in the first and second order of perturbation theory that can nonradiatively

decay into the exciton state and reduce the absorption of the exciton state in third order (indirect exciton saturation), as shown in Fig. 3(a). The second nonlinear term represents direct nonlinear absorption of the excitons in which the pump and probe beam excites an exciton population in first and second order that directly saturates the absorption of the probe beam in third order, as shown in Fig. 3(b) (direct exciton saturation).

In Fig. 3(c), we plot the theoretical direct and indirect saturation components (red and blue lines) as well as the total nonlinear signal expected from the theory presented in the Supplemental Material [21] [green line—representing the imaginary part of Eq. (S9)] assuming that $\Gamma_{\mathrm{Dec}} = 10\Gamma_X$, where Γ_{Dec} is the rate of exciton decoherence and Γ_X is the exciton population decay rate [21,32]. At zero pump-probe detuning (both pump and probe are resonant with the exciton state), the direct term shows a resonance while the indirect term shows a monotonically increasing signal as a function of pump energy that follows the same dependence as the exponential PLE signal for $\omega_{\mathrm{pump}} > \omega_{\mathrm{probe}}$. If both the direct and indirect saturation terms contribute equally, the signal shows a peak at zero pump-probe detuning that is skewed by the exponential density of states term.

The nondegenerate CPP data in Fig. 1(b) show no evidence of resonant structures that are characteristic of the direct exciton excitation response from Fig. 3(c). Instead, the data indicate that the nonlinear response is mostly dominated by the indirect saturation term that results in a monotonic increase in signal as a function of pump energy with respect to the fixed probe energy. Indeed, the nondegenerate CPP signal for $\hbar\omega_{\mathrm{probe}} = 1.95$ eV, nearly on resonance with an exciton transition from the DCPP data shown in Fig. 1(b), shows a good fit to the indirect exciton saturation response as shown in Fig. 1(c) [first term on the right-hand side of Eq. (S9)] in addition to the negative dT/T offset. From the fit, we estimate the homogeneous linewidth of the exciton state to be $\sim$15 meV, consistent with previous reports at room temperature [30]. Large decoherence rates of excitons at low temperature in InGaN have been observed before [26] and attributed to effects such as disorder-induced dephasing [35]. For this system, the fit in Fig. 1(c) can provide similar information to spectral hole burning [32] of the inhomogeneously broadened exciton ensemble. The dominance of the indirect saturation term over the direct term indicates that the rate of nonradiative population transfer of electron-hole pairs from the disorder states into the excitons largely exceeds both the direct optical pumping rate into the exciton state from the pump beam and the total decay rate of the exciton Γ_X. It is also possible that population transfer from exciton excited states to lower-energy exciton states, such as by Förster [36] or Dexter [37] energy transfer, can add to the dT/T signal. This would likely lead to additional resonances in the nondegenerate CPP response at higher pump energies compared to the probe that reflects the density of exciton excited states that may be visible in measurements such as DCPP. It is possible that the slight dip in the nondegenerate data near 2.10 eV is due to this type of coupling, but further validation will be needed in future studies at the single DINW level.

To further show consistency between the data and the above model, we fit the DCPP signal from Fig. 1(b) using the indirect saturation response with $\omega_{\mathrm{pump}} = \omega_{\mathrm{probe}}$, which assumes that the indirect term is dominant over the direct term. We find that the value for the exponential decay constant $\frac{1}{\omega_0}$ from Eqs. (S9) and (S10) in the Supplemental Material [21] extracted from the fit (0.076 ± 0.005) shows some discrepancy from a single exponential fit to the PLE data shown in Fig. 1(a), where $\frac{1}{\omega_0} = 0.109 \pm 0.003$. This discrepancy is possibly related to an incomplete knowledge of the exciton energy distribution in the system, resulting in a fit in Fig. 1(b) with too few resonances. It is also possible that the fit can be influenced by higher-energy transitions outside of the laser tuning range. Shown for reference in Fig. 1(b) is the nonlinear absorption from the exciton transitions in the absence of disorder state coupling (i.e., the direct excitation term).

In summary, the above results indicate that optical excitation of the sample results in a steady-state lowest-order (second order in the applied field) exciton population that is primarily populated via nonradiative coupling from higher-energy disorder states. As discussed in the Supplemental Material [21], we expect the PL brightness to scale as $N\Gamma_{XR}$ for high excitation intensities, where N is proportional to the total population of disorder states that are coupled to the exciton and Γ_{XR} is the radiative decay rate of the exciton. This shows that the emission efficiency of InGaN DINWs at high excitation intensities might be improved by the incorporation of disorder in the system. This Rapid Communication provides an important glimpse into the dynamics of optically excited electron-hole pairs in InGaN systems. Since InGaN layers in other device structures such as planar quantum wells are known to contain a large density of localized disorder states [17], we believe that the decay of optically excited electron-hole pairs from disorder states into the excitons should be generally incorporated into future materials modeling and engineering design of InGaN layers.

This work was funded at the University of Michigan through NSF:CPHOM (DMR 1120923).

[1] T. Mukai, M. Yamada, and S. Nakamura, Jpn. J. Appl. Phys. **38**, 3976 (1999).
[2] L. Zhang, L.-K. Lee, C.-H. Teng, T. A. Hill, P.-C. Ku, and H. Deng, Appl. Phys. Lett. **104**, 051116 (2014).
[3] H. Y. Ryu, K. S. Jeon, M. G. Kang, H. K. Yuh, Y. H. Choi, and J. S. Lee, Sci. Rep. **7**, 44814 (2017).
[4] S. Nakamura, T. Mukai, and M. Senoh, J. Appl. Phys. **76**, 8189 (1994).
[5] I. Akasaki and H. Amano, Jpn. J. Appl. Phys. **36**, 5393 (1997).
[6] M. Auf der Maur, A. Pecchia, G. Penazzi, W. Rodrigues, and A. Di Carlo, Phys. Rev. Lett. **116**, 027401 (2016).
[7] W. Guo, M. Zhang, A. Banerjee, and P. Bhattacharya, Nano Lett. **10**, 3355 (2010).
[8] S. D. Hersee, A. K. Rishinaramangalam, M. N. Fairchild, L. Zhang, and P. Varangis, J. Mater. Res. **26**, 2293 (2011).

[9] F. Sacconi, M. A. der Maur, and A. D. Carlo, IEEE Trans. Electron Devices **59**, 2979 (2012).
[10] T. Frost, S. Jahangir, E. Stark, S. Deshpande, A. Hazari, C. Zhao, B. S. Ooi, and P. Bhattacharya, Nano Lett. **14**, 4535 (2014).
[11] A. Hazari, A. Aiello, T.-K. Ng, B. S. Ooi, and P. Bhattacharya, Appl. Phys. Lett. **107**, 191107 (2015).
[12] Y.-H. Ra, R. Wang, S. Y. Woo, M. Djavid, S. M. Sadaf, J. Lee, G. A. Botton, and Z. Mi, Nano Lett. **16**, 4608 (2016).
[13] H. P. T. Nguyen, M. Djavid, S. Y. Woo, X. Liu, A. T. Connie, S. Sadaf, Q. Wang, G. A. Botton, I. Shih, and Z. Mi, Sci. Rep. **5**, 7744 (2015).
[14] C. Zhao, T. K. Ng, R. T. ElAfandy, A. Prabaswara, G. B. Consiglio, I. A. Ajia, I. S. Roqan, B. Janjua, C. Shen, J. Eid, A. Y. Alyamani, M. M. El-Desouki, and B. S. Ooi, Nano Lett. **16**, 4616 (2016).
[15] S. Deshpande, T. Frost, L. Yan, S. Jahangir, A. Hazari, X. Liu, J. Mirecki-Millunchick, Z. Mi, and P. Bhattacharya, Nano Lett. **15**, 1647 (2015).
[16] L. Zhang, C.-H. Teng, T. A. Hill, L.-K. Lee, P.-C. Ku, and H. Deng, Appl. Phys. Lett. **103**, 192114 (2013).
[17] C. J. Humphreys, Philos. Mag. **87**, 1971 (2007).
[18] G. H. Gu, D. H. Jang, K. B. Nam, and C. G. Park, Microsc. Microanal. **19**, 99 (2013).
[19] S. F. Chichibu, A. Uedono, T. Onuma, B. A. Haskell, A. Chakraborty, T. Koyama, P. T. Fini, S. Keller, S. P. DenBaars, J. S. Speck, U. K. Mishra, S. Nakamura, S. Yamaguchi, S. Kamiyama, H. Amano, I. Akasaki, J. Han, and T. Sota, Nat. Mater. **5**, 810 (2006).
[20] C. Nelson, S. Deshpande, A. Liu, S. Jahangir, P. Bhattacharya, and D. G. Steel, J. Opt. Soc. Am. B **34**, 1206 (2017).
[21] See Supplemental Material at http://link.aps.org/supplemental/10.1103/PhysRevB.98.081201 for more details on the sample growth procedure, nonlinear spectroscopy measurement techniques, and theoretical analysis of the nonlinear and intensity-dependent PL spectra.
[22] Y.-H. Ra, T. R. Rashid, X. Liu, J. Lee, and Z. Mi, Adv. Funct. Mater. **27**, 1702364 (2017).
[23] F. Urbach, Phys. Rev. **92**, 1324 (1953).
[24] R. W. Martin, P. G. Middleton, K. P. O'Donnell, and W. Van der Stricht, Appl. Phys. Lett. **74**, 263 (1999).
[25] M. Piccardo, C.-K. Li, Y.-R. Wu, J. S. Speck, B. Bonef, R. M. Farrell, M. Filoche, L. Martinelli, J. Peretti, and C. Weisbuch, Phys. Rev. B **95**, 144205 (2017).
[26] D. O. Kundys, J.-P. R. Wells, A. D. Andreev, S. A. Hashemizadeh, T. Wang, P. J. Parbrook, A. M. Fox, D. J. Mowbray, and M. S. Skolnick, Phys. Rev. B **73**, 165309 (2006).
[27] N. H. Bonadeo, A. S. Lenihan, G. Chen, J. R. Guest, D. G. Steel, D. Gammon, D. S. Katzer, and D. Park, Appl. Phys. Lett. **75**, 2933 (1999).
[28] H. Haug and S. W. Koch, *Quantum Theory of the Optical and Electronic Properties of Semiconductors*, 5th ed. (World Scientific, Singapore, 2014).
[29] M. Kira and S. W. Koch, *Semiconductor Quantum Optics* (Cambridge University Press, New York, 2012).
[30] C. Nelson, Y.-H. Ra, Z. Mi, P. Berman, and D. G. Steel, Phys. Rev. B **96**, 115302 (2017).
[31] H. Schömig, S. Halm, A. Forchel, G. Bacher, J. Off, and F. Scholz, Phys. Rev. Lett. **92**, 106802 (2004).
[32] P. R. Berman and V. Malinovsky, *Principles of Laser Spectroscopy and Quantum Optics* (Princeton University Press, Princeton, NJ, 2010).
[33] C. Gourdon and P. Lavallard, J. Cryst. Growth **101**, 767 (1990).
[34] T. Takagahara, Phys. Rev. B **60**, 2638 (1999).
[35] C. Lonsky, P. Thomas, and A. Weller, Phys. Rev. Lett. **63**, 652 (1989).
[36] V.T. Förster, Z. Naturforsch. **4A**, 321 (1949).
[37] D. L. Dexter, J. Chem. Phys. **21**, 836 (1953).